RSC Advances

PAPER

View Article Online
View Journal | View Issue

Cite this: *RSC Adv.*, 2021, **11**, 26502

A study on the high efficiency reduction of *p*-nitrophenol (4-NP) by a $Fe(OH)_3/Fe_2O_3$@Au composite catalyst†

Meirong Fu, Mingqiang Li, Yingying Zhao, Yunxiang Bai, Xingzhong Fang, Xiaolong Kang, Min Yang, Yanping Wei and Xia Xu *

Received 25th May 2021
Accepted 16th July 2021

DOI: 10.1039/d1ra04073a

rsc.li/rsc-advances

Precious metal nanometric catalysts are widely used in the removal of harmful substances. In the process of synthesis and catalytic reaction, it is particularly important to study green and simple synthesis methods and high catalytic efficiency. In this paper, a green one-step method was used to synthesize the $Fe(OH)_3/Fe_2O_3$@Au composite catalyst, in which Au was single atom-dispersed. The removal of 4-nitrophenol (4-NP), a typical dangerous chemical widely existing in factory waste gas, waste water and automobile exhaust gas, was catalysed by $Fe(OH)_3/Fe_2O_3$@Au. The catalytic performance of $Fe(OH)_3/Fe_2O_3$@Au with different synthesis conditions (different amounts of MES, $NaBH_4$, $FeSO_4$, Au and Pt) on the 4-NP reduction reaction were systematically studied. Finally, the stability and recyclability of $Fe(OH)_3/Fe_2O_3$@Au composite nanocatalyst were investigated thoroughly.

Introduction

In recent decades, precious metal nanomaterials, especially Au, Pt, and Pd, are attracting much attention due to their unique physical and chemical properties, and a wide range of high-activity catalysts. So far, precious metal nanomaterials have been widely used in various fields, such as hydrogenation reactions, hydrolysis reactions, fuel cells, and electrocatalytic reactions.[1–8] In particular, precious metal nanoparticles exhibit superior catalytic performance due to their unique functional mechanism and synergistic effect of electronic effects.[9–11] Moreover, it has remarkable activity for the reduction of 4-nitrophenol (4-NP).

With the advancement of time, the emission of pollutants from industrial refineries, automobile exhaust and organic pollutants from various factories have become an urgent environmental problem. The organic pollutants released contain 4-NP, which are toxic, non-biodegradable and highly persistent in the environment, thus being listed as a priority toxic pollutant by the US Environmental Protection Agency (EPA).[12–14] The reduction product of 4-NP is 4-AP, which has significantly lower toxicity and is an important chemical intermediate in the synthesis of pesticides, dyes, imaging agents, and drugs (such as paracetamol).[14] Hence, it has become an important research field to obtain 4-AP and similar derivatized aminophenols by the mild aqueous phase catalytic reduction of 4-NP.[15,16] Therefore, it is necessary to develop environmentally compatible, cost-effective and easy to recycle effective composite nanomaterials to degrade toxic 4-NP into 4-AP.

Among all reported precious metal nanoparticles, Pt and Au nanoparticles are particularly attractive for the 4-NP reduction reaction.[17–19] Many precious metals with different structures and compositions have been extensively studied, and have shown excellent catalytic performance.[20–22] However, the stability of the application of precious metals is still a common problem due to the tendency of precious metals to aggregate, which leads to a gradual decline in catalytic activity.[23] In addition, it is difficult to separate and recover precious metal nanoparticles after each use due to their small size. Moreover, the cost of precious metals is very high, and better separation and recovery are very important under the shortage of resources and huge industrial demand.

In order to overcome these problems, various strategies have been attempted to improve the catalytic performance and stability of precious metal nanoparticles. In recent years, many research studies have been focused on the synthesis of various precious metal composite materials,[24–26] and the improvement of their catalytic activity and stability. For example, Au–Pt alloy nanoparticles are loaded on α-$Co(OH)_2$ nanosheets to improve the catalytic performance for the 4-NP reduction reaction.[26] In addition cinchonidine is used as a catalyst to catalyze the synthesis of well-dispersed ultrafine palladium nanoparticles with high catalytic activity.[27] The synthesis of the CeO_2@-Au@CeO_2–MnO_2 sandwich hollow structure improves the catalytic performance.[28] In addition, transition metal oxides are widely used in catalysis. For example, in nano-CeO_2 doped with high silicon ZSM-5, the derivatives Co_3O_4/C and Co_3O_4–C@FeOOH catalyze ozonization in water.[29–31] The $CuCo_2O_4$/

College of Science, Gansu Agricultural University, No. 1 Yingmen Village, Lanzhou 730070, P. R. China. E-mail: xuxia@gsau.edu.cn

† Electronic supplementary information (ESI) available. See DOI: 10.1039/d1ra04073a

$BiVO_4$ composite material effectively catalyzed the 4-NP reduction in water.[32] Further, the synthesis of silver-doped Fe_3O_4/C nanoparticles and its catalytic activities are applied for the degradation and reduction of methylene blue and 4-nitrophenol.[33] As mentioned above, these all indicate that the composite catalysts based on precious metals or transition metal oxide have a good catalytic effect on the 4-NP reduction reaction, and the catalytic activity and stability of these composite materials have been improved.

For composite catalysts based on precious metals, precious metals are usually connected to the supporting material through a weak interaction provided by a special linker. However, most synthesis methods need to synthesize the carrier material first, and then load the metal nanoparticles. The synthesis process is complicated and time-consuming.[34–37] Among all the support materials, graphene with unique structures and properties, as well as various modified graphenes, are the most widely used. Like graphene, ultra-thin nanosheets with a thickness of a few nanometers is rich in active sites for ions and electrons. It also has a shorter diffusion path length and a higher specific surface area. Taking advantage of these advantages, ultrathin nanosheets will be a promising new two-dimensional support material for supporting precious metal nanoparticles. Although the larger specific surface area and stability of ultrathin nanosheets in water help improve the stability of precious metal nanoparticles, there is no specific metal ligand on ultrathin nanosheets. Therefore, in order to further improve the stability of Au NPs, it is necessary to introduce metal binding groups on the surface of nanosheets. By consulting the literature, it is found that polyvinyl pyrrolidone (PVP) and morpholine ethanesulfonic acid (MES) have good metal affinity, especially MES.[38–41] Therefore, PVP and MES can be used as stabilizers of Au NPs to form complexes with $Fe(OH)_3/Fe_2O_3$ nanosheets.[40]

In this study, single atom-dispersed Au nanoparticles were loaded on the support material of ultra-thin $Fe(OH)_3/Fe_2O_3$ nanosheets *via* a green one-step method. The catalytic efficiency of the $Fe(OH)_3/Fe_2O_3$@Au composite nanomaterials under different synthesis conditions for 4-NP reduction was explored. Finally, the catalytic activity and stability of the prepared nanocomposite were systematically investigated.

Experimental

Materials

Tetrachloroauric acid trihydrate ($HAuCl_4 \cdot 3H_2O$ 1 g/100 mL), polyvinyl pyrrolidone (PVP, $M_w = 58\,000$), morpholine ethanesulfonic acid (MES, $M_w = 195.24$), and *p*-nitrophenol (4-NP) (>99.0%) were purchased from Shanghai Aladdin Biochemical Technology Co., Ltd. Sodium borohydride ($NaBH_4$) and ferrous sulfate ($FeSO_4$) were purchased from Beijing Chemical Plant. The purity of all reagents was analytically pure, and all chemicals were bought directly without any purification.

Synthesis of the $Fe(OH)_3/Fe_2O_3$ composite nanomaterials

The specific experimental steps are as follows: first, 100 mg PVP and 200 mg MES were dissolved in 30 mL deionized water. Subsequently, while vigorously stirring, 5 mg $FeSO_4$ was quickly injected, then stirring was continued for 5 min. Moreover, 30 mg $NaBH_4$ was quickly added while stirring vigorously, and continued stirring for 30 min. The entire reaction process is carried out at room temperature. Finally, the product was separated by centrifugation (10 000*g*, 10 min), and dispersed in 2 mL deionized water for later use.

Synthesis of the $Fe(OH)_3/Fe_2O_3$@Au composite nanomaterials

The specific experimental steps are as follows: first, 0.3 mL $HAuCl_4 \cdot 3H_2O$, 100 mg PVP and 200 mg MES were dissolved in 30 mL deionized water. Subsequently, while vigorously stirring, 0.5 mL of a freshly prepared 6 mg mL^{-1} $NaBH_4$ aqueous solution and 5 mg $FeSO_4$ were quickly injected, and then stirring was continued for 5 min. Moreover, 30 mg $NaBH_4$ was quickly added while stirring vigorously, and continued stirring for 30 min. A tan solution could then be observed. The entire reaction process was carried out at room temperature. Finally, the product was separated by centrifugation (10 000*g*, 10 min), and dispersed in 2 mL deionized water for later use. The synthesis method of the $Fe(OH)_3/Fe_2O_3$@Au composite nanomaterials with different amounts of MES, $NaBH_4$, $FeSO_4$ was the same, with the other conditions remaining unchanged, and only the additional amount of MES (0, 100, 200 mg), and $NaBH_4$ (0.5, 1.5, 3 mg) and $FeSO_4$ (3, 5, 7 mg) added in the synthesis process were changed.

The sample's catalytic performance test for 4-NP reduction reaction

The catalytic reaction was carried out at room temperature with a 4 mL quartz colorimetric dish as the reaction vessel. The absorbance of the solution during the reaction was monitored by UV-Vis spectra and 722N visible spectrophotometer, respectively. The specific operation steps are as follows: first, fresh 4-NP (0.01 mol L^{-1}) and $NaBH_4$ (0.2 mol mL^{-1}) aqueous solutions were prepared, and the catalyst was dispersed into deionized water to form a 1.3 mg mL^{-1} dispersion solution. In a 4 mL quartz colorimetric dish, 20 μL 4-NP (0.01 mol L^{-1}), 3 mL H_2O and 10 μL catalyst solution (1.3 mg mL^{-1}) were successively added. After the solution was completely and evenly dispersed, 100 μL $NaBH_4$ (0.2 mol L^{-1}) aqueous solution was dropped into the above solution. Then, the UV-vis spectrum was scanned in the range of 250–600 nm immediately, or the absorbance value was record at $\lambda = 400$ nm.

Recycling ability test

In order to investigate the stability of $Fe(OH)_3/Fe_2O_3$@Au, we conducted 3 cycles of $Fe(OH)_3/Fe_2O_3$@Au and measured the conversion rate of 4-NP within the same reaction conditions. In order to avoid the loss of catalyst caused by the separation process, 20 μL of 4-NP solution was directly added to the reaction system after each reaction, and then the next test was performed.

Characterization

The crystal structure and phase purity of the samples were measured by a Panaco X'Pert PRO X-ray diffractometer. A

Panalytical Empyrean powder X-ray Cu-Kα radiation diffractometer with wavelength set to 0.15406 nm, commonly used voltage at 45 kV, current at 40 mA, and scanning speed: 2° min^{-1}, was used for measurement in the following test range: $10^\circ \leq 2\theta \leq 70^\circ$. The elemental composition of the $Fe(OH)_3$/Fe_2O_3@Au nanocomposites was determined by Zeiss MERLIN Compact SEM-EDX microanalysis. The chemical states of different elements were determined by Thermo ESCALAB 250XI X-ray photoelectron spectroscopy (XPS). TEM images of the samples were obtained on a FEI Talos F200S transmission electron microscope (acceleration voltage: 200 kV). The UV-Vis absorption spectra of the samples were measured on a Shimadzu UV-1780 UV-vis-NIR spectrophotometer. The absorbance of the solution during the reaction was monitored by a 722N visible spectrophotometer.

Results and discussions

Analysis of the morphology, crystalline phase, and chemical composition of the $Fe(OH)_3/Fe_2O_3$@Au composite nanocatalyst

The chemical composition, crystalline phase and the morphology of the prepared $Fe(OH)_3/Fe_2O_3$@Au nanocomposite were characterized by XPS, XRD, EDX and TEM. First, the electronic states of Au and Fe in the $Fe(OH)_3/Fe_2O_3$@Au composite nanomaterials were determined by XPS technique. As shown in Fig. 1a, the high-resolution Au 4f peaks near the binding energies of 83.5 and 87.1 eV confirm the zero valent Au element, and the main peaks are attributed to Au $4f_{7/2}$ and Au $4f_{5/2}$, respectively. The Fe 2p spectrum has two peaks at the binding energies of 711.0 and 725.2 eV (Fig. 1b), and the main peaks are attributed to Fe $2p_{3/2}$ and Fe $2p_{1/2}$, respectively. The Fe 2p spectrum indicates that Fe exists in the form of a positive trivalent. Two shake satellites with Fe^{3+} were found in the XPS spectra of Fe 2p. Fig. S1† shows the chemical composition and crystalline phase of the synthesized $Fe(OH)_3/Fe_2O_3$@Au nanocomposite characterized by X-ray diffraction (XRD). The obvious diffraction peaks of $Fe(OH)_3$ at $2\theta = 14.2^\circ$, 36.4°, 46.9° and 59.1° are well indexed on the $Fe(OH)_3$ standard card (JCPDS no. 38-0032). The obvious diffraction peaks of face-centered cubic crystalline Fe_2O_3 at $2\theta = 26.9^\circ$, 36.2°, 48.9° and 54.9° are well indexed on the (002) (020) (113) and (004) planes, respectively, of the standard face-centered cubic crystalline Fe_2O_3 card (JCPDS no. 34-0394). The diffraction peak at $2\theta = 38.2^\circ$ has a good index to the (111) plane of the face-centered cubic crystalline Au. Therefore, the XPS spectra and XRD results show that the synthesized composite nanomaterials are the $Fe(OH)_3$/Fe_2O_3@Au nanocomposite. In addition, the broad diffraction peaks indicate that the size of the Au nanoparticles is smaller. The EDX spectrum also confirmed the existence of Au, O and Fe in the $Fe(OH)_3/Fe_2O_3$@Au nanomaterials (as shown in Fig. S2†).

As shown in Fig. 2, the morphology and size of the synthesized $Fe(OH)_3/Fe_2O_3$@Au nanocomposite were characterized by transmission electron microscopy (TEM). It can be clearly seen that $Fe(OH)_3/Fe_2O_3$ is distributed in space as ultrathin sheets, and the lateral dimensions of the $Fe(OH)_3/Fe_2O_3$ sheets range from hundreds of nanometers to thousands of nanometers. The Au nanoparticles, about 10 nm in diameter, are randomly distributed on the ultrathin $Fe(OH)_3/Fe_2O_3$ sheets. In order to optimize the experimental conditions, MES was added to the reaction system. When 200 mg MES is added, the morphology and size of the $Fe(OH)_3/Fe_2O_3$@Au nanocomposite change greatly. As shown in Fig. 2(d)–(f), the $Fe(OH)_3/Fe_2O_3$ nanosheets become smaller and thinner, and the dispersion is better. The single atom-dispersed Au nanoparticles loaded on the $Fe(OH)_3$/Fe_2O_3 nanosheets have increased in number and become smaller in size (Fig. 2f). Because MES has good metal affinity, the addition of MES can coordinate with Au nanoparticles and act as a stabilizer for these nanoparticles.[38,39]

On this basis, the possible formation mechanism of $Fe(OH)_3/Fe_2O_3$@Au is proposed. In previous reports, Zhang and colleagues have demonstrated that there is a key reaction intermediate in the formation of ultra-thin α-$Co(OH)_2$ nanosheets-Co–B composite nanospheres.[42] When M^{2+} (M = Fe, Co, Ni) salt and $NaBH_4$ are mixed in deionized water in the presence of PVP, a solution of M–B nanospheres composed of small metal crystals embedded in an amorphous boron matrix is formed. Then, through the oxidation of the metal in the air and the release of the boron species at the same time, the M–B composite material becomes an ultra-thin nanosheet.[31] Presumably, the same process applies here. The newly prepared $NaBH_4$ solution was injected into a solution containing Au nanoparticles, $FeSO_4$, PVP and MES, and Fe^{2+} was reduced to form a Fe–B composite solution immediately. Then, the reaction system was gradually transformed into ultra-thin $Fe(OH)_3$/

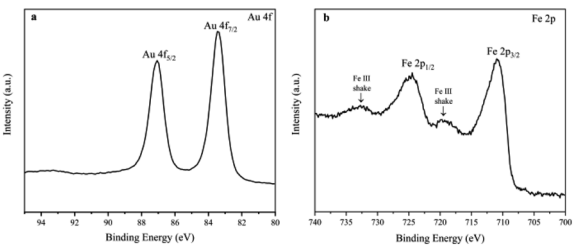

Fig. 1 XPS fine spectra of $Fe(OH)_3/Fe_2O_3$@Au: (a) Au 4f spectra and (b) Fe 2p spectra.

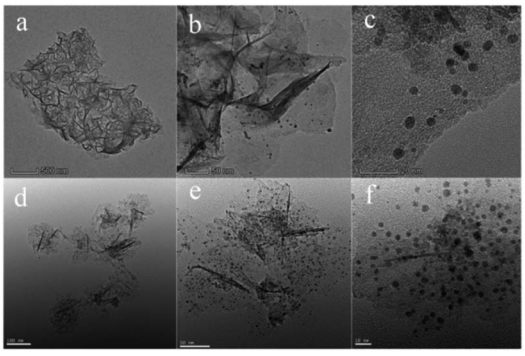

Fig. 2 Transmission electron microscopy (TEM) images of the $Fe(OH)_3/Fe_2O_3$@Au composite nanocatalyst under different reaction conditions: (a)–(c) 0 mg MES; (d)–(f) 200 mg MES.

Fe_2O_3@Au through an oxidation corrosion process. In addition, PVP and MES have good metal affinity and can coordinate with Au nanoparticles, and act as stabilizers for these nanoparticles. It is these multiple interactions that connect Au NPs with ultrathin $Fe(OH)_3/Fe_2O_3$ nanosheets and stabilize the prepared $Fe(OH)_3/Fe_2O_3$@Au.

Study on the catalytic performance of $Fe(OH)_3/Fe_2O_3$@Au

Like other aromatic nitro compounds, 4-nitrophenol is a dangerous and carcinogenic chemical, which is the main component of pesticides, plasticizers and herbicides.[37] Simultaneously, 4-aminophenol (4-AP) is an important intermediate in the industrial production process, including the production of analgesics and antiseptic lubricants.[43–45] The development of efficient methods for reducing nitro groups to amino groups using new catalysts has attracted great attention in synthetic organic chemistry.[46–49] In the field of catalysis, the reduction of 4-NP to 4-AP has been widely used as a benchmark system for evaluating the catalytic ability of metal-based materials.[50] The reaction was carried out in an aqueous solution at room temperature to evaluate the catalytic capacity of prepared $Fe(OH)_3/Fe_2O_3$@Au. Ultraviolet-visible spectroscopy was used to monitor the catalytic reaction process in the range of 200–600 nm.

The $Fe(OH)_3/Fe_2O_3$@Au at a concentration of 4.4 μg mL^{-1} reduces the ultraviolet-visible spectrum of 4-NP in the aqueous solution (as shown in Fig. 3). As shown in Fig. 3, after mixing 4-NP and $NaBH_4$, a strong absorption peak of 4-NP centered at 400 nm appears. As the reduction of 4-NP is catalyzed by $Fe(OH)_3/Fe_2O_3$@Au, the intensity of the absorption peak centered at 400 nm gradually decreases, and a new absorption peak appears at 300 nm, which is caused by 4-AP. In just 110 s, the absorption peak centered at 400 nm disappeared fully, indicating that 4-NP was completely catalyzed and converted to 4-AP (as shown in Fig. 3). Since the amount of $NaBH_4$ is excessive, the reaction is believed to follow the quasi-first order kinetics of 4-nitrophenol.[44,45,51] These results show that $Fe(OH)_3/Fe_2O_3$@Au catalyst has high catalytic activity to the 4-NP reduction reaction, and it is further confirmed that the $Fe(OH)_3/Fe_2O_3$@Au catalyst can convert 4-NP to 4-AP. Compared with other literature studies, it was found that the catalytic activity of $Fe(OH)_3/Fe_2O_3$@Au (4.4 μg mL^{-1}) was much higher than that of other similar catalysts with only a fraction of the $Fe(OH)_3/Fe_2O_3$@Au catalyst concentration.[52–56] For example, the catalytic reduction of the same amount of 4-nitrophenol with 2.5 mg mL^{-1} Au/$CaCO_3$ nanocomposite takes 3 min,[52] the 1.0 mmol mL^{-1} Au@S–g-C_3N_4 nanocomposite takes 5 min,[53] and 6 mg eggshell/Ag takes 5 min.[54] Nevertheless, with 4.4 μg mL^{-1}, $Fe(OH)_3/Fe_2O_3$@Au takes only 110 s.

Catalyst activity under different conditions

In order to facilitate the detection of the 4-NP reduction reaction catalysed by the $Fe(OH)_3/Fe_2O_3$@Au composite, we estimated the 4-NP ion concentration by recording the absorbance value at the wavelength of 400 nm *via* 722N visible spectrophotometer. First, the catalytic activity of $Fe(OH)_3/Fe_2O_3$@Au with different concentrations on the reduction of 4-NP were investigated. A series of $Fe(OH)_3/Fe_2O_3$@Au with different concentrations (2.2 μg mL^{-1}, 4.4 μg mL^{-1}, 6.6 μg mL^{-1} and 8.8 μg mL^{-1}) were selected for the experiment. As shown in Fig. 4, when the catalyst is added to the reaction mixture, the reduction reaction begins to take place after a period of time, which can be called the plateau phase. According to previous literature, 4-NP ions can only be reduced by adsorption of active hydrogen converted by $NaBH_4$. That is to say, the reaction will only occur when 4-NP and BH_4^- are adsorbed on the surface of the catalyst at the same time.[51] Therefore, we believe that the time required for BH_4^- to absorb on the catalyst surface, and evolve into active H-atoms is a key component of the induction period. Since $NaBH_4$ is excessive in the reaction system, catalytic reduction of 4-NP can be regarded as a quasi-first order reaction in terms of the concentration of 4-NP. Therefore, dynamic information can be obtained according to eqn (1) and (2):[57]

$$-\mathrm{d}c/\mathrm{d}t = K_{\mathrm{app}} \times c \quad (1)$$

$$\ln(c/c_0) = -K_{\mathrm{app}} \times t \quad (2)$$

where c is the concentration of 4-NP, t is the reaction time, K_{app} is the apparent reaction rate, and c_0 is the initial concentration of 4-NP.

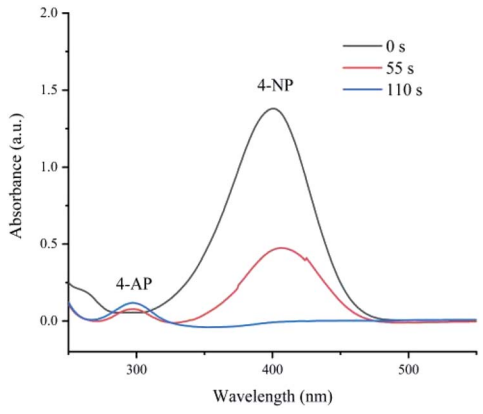

Fig. 3 Time-dependent UV-Vis absorption spectra of the reduction of 4-NP catalyzed by $Fe(OH)_3/Fe_2O_3$@Au.

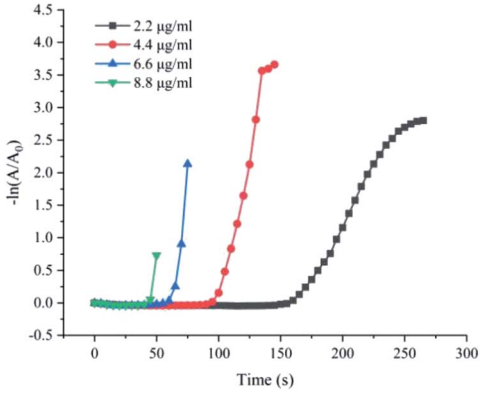

Fig. 4 Plots of $-\ln(A/A_0)$ *versus* the reaction time t for the reduction of 4-NP catalyzed by different dosages of $Fe(OH)_3/Fe_2O_3$@Au aqueous solution (2.2, 4.4, 6.6 and 8.8 μg mL^{-1}).

In Fig. 4, the slope of the straight line represents the reaction rate of the 4-NP reduction reaction, which is K_{app}. There is no doubt that the greater the catalyst concentration, the shorter the plateau period and the faster the reaction rate. At the same time, as the catalyst concentration increases, K_{app} first increases and then tends to be constant. However, in order to continue optimizing the experimental conditions, the concentration of all catalysts selected in the subsequent tests was 4.4 μg mL^{-1}. Then, we compared the catalytic activity of $Fe(OH)_3/Fe_2O_3$@Au with $Fe(OH)_3/Fe_2O_3$. As shown in Fig. S3,† $Fe(OH)_3/Fe_2O_3$ has no catalytic activity at all. However, $Fe(OH)_3/Fe_2O_3$@Au has high catalytic efficiency when the Au nanoparticles are loaded on the surface of the ultrathin $Fe(OH)_3/Fe_2O_3$ nanosheets. Secondly, the effects of different MES supplemental levels (0 mg, 100 mg and 200 mg) on the reduction activity of 4-NP were investigated. As shown in Fig. 5a, the good linear relationship between $-\ln(A/A_0)$ and reaction time t confirmed the apparent quasi-first order kinetics. The K_{app} could be given from the slope of $-\ln(A/A_0)$ *versus* time t plots. When 200 mg MES is added, the catalytic activity is the highest, which corresponded to the TEM results. As shown in Fig. 2d, when 200 mg MES is added, the $Fe(OH)_3/Fe_2O_3$ nanosheets become smaller and thinner, and the dispersion is better. The single atom-dispersed Au nanoparticles loaded on the $Fe(OH)_3/Fe_2O_3$ nanosheets have increased in number and become smaller in size. Therefore, more active sites are exposed and the catalytic activity is better. So, the amount of MES was fixed to 200 mg in the following experiments.

In addition, the effects of different $NaBH_4$ supplemental levels (0.5 mg, 1.5 mg and 3.0 mg) on the reduction activity of 4-NP in the initial step were investigated. As shown in Fig. 5b, the more $NaBH_4$ supplemental levels, the longer the plateau period. The linear relationship between $-\ln(A/A_0)$ and the reaction time t indicates that the $Fe(OH)_3/Fe_2O_3$@Au nanocomposite has the strongest reduction activity for 4-NP when 0.5 mg $NaBH_4$ is added. It may be that when the amount of $NaBH_4$ is small, the reduced Au nanoparticles have a smaller size, larger specific

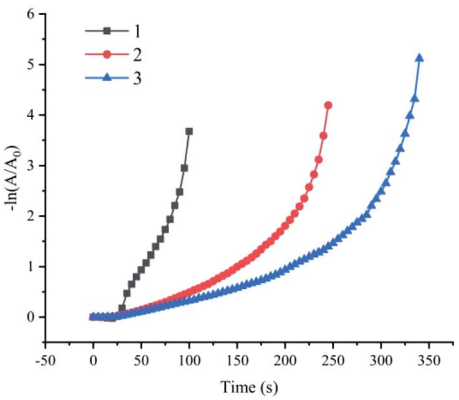

Fig. 6 The reusability of $Fe(OH)_3/Fe_2O_3$@Au for three cycles of 4-NP reduction reaction.

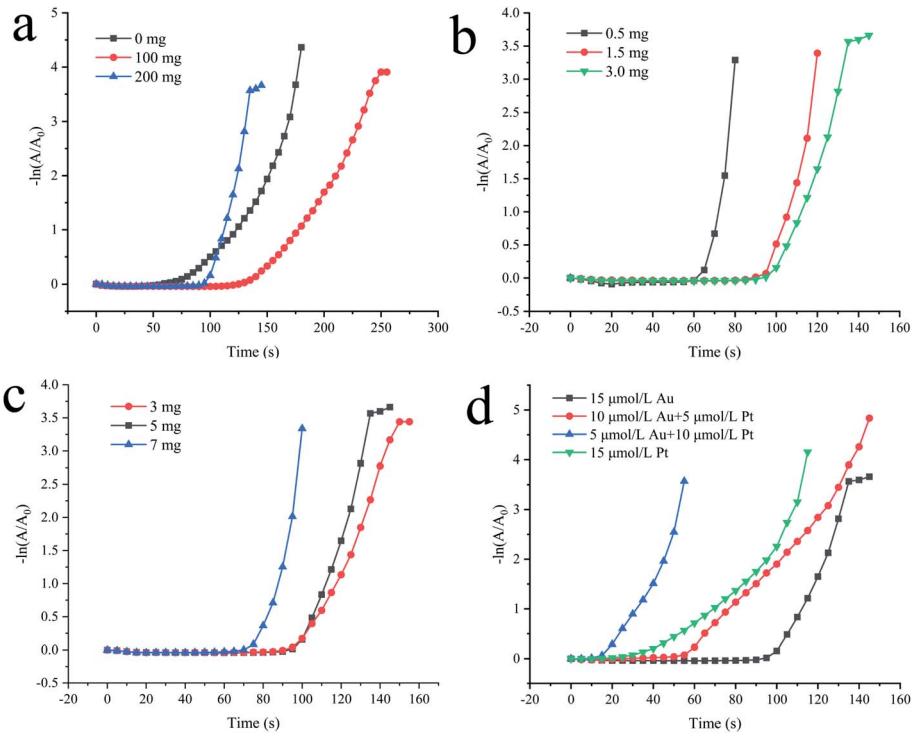

Fig. 5 Plots of $-\ln(A/A_0)$ *versus* the reaction time t for the reduction of 4-NP catalyzed by $Fe(OH)_3/Fe_2O_3$@Au with (a) different amounts of MES: 0 mg MES, 100 mg MES and 200 mg MES, respectively, (b) different amounts of $NaBH_4$: 0.5 mg $NaBH_4$, 1.5 mg $NaBH_4$ and 3.0 mg $NaBH_4$, respectively, (c) different amounts of $FeSO_4$: 3 mg $FeSO_4$, 5 mg $FeSO_4$, and 7 mg $FeSO_4$, respectively. (d) Plots of $-\ln(A/A_0)$ *versus* the reaction time t for the reduction of 4-NP catalyzed by the $Fe(OH)_3/Fe_2O_3$@Au, $Fe(OH)_3/Fe_2O_3$@$Au_{2/3}/Pt_{1/3}$, $Fe(OH)_3/Fe_2O_3$@$Au_{1/3}/Pt_{2/3}$ and $Fe(OH)_3/Fe_2O_3$@Pt nanocomposites.

surface area and more active sites, so the catalytic activity is stronger.

Then, the effects of different $FeSO_4$ additions (3 mg, 5 mg and 7 mg) on the reduction activity of 4-NP were explored (as shown in Fig. 5c). The more $FeSO_4$ is added, the more $Fe(OH)_3/Fe_2O_3$ nanosheets are formed under the same conditions. The faster 4-NP and BH_4^- are simultaneously adsorbed on the catalyst surface. Therefore, under the same conditions, the more $FeSO_4$ content, the shorter the plateau period of adsorption (as shown in Fig. 5c). At the same time, the good linear relationship between $-\ln(A/A_0)$ and reaction time t confirmed the apparent quasi-first order kinetics (Fig. 5c). It can also be found from Fig. 5c that the more $FeSO_4$ is added, the stronger the reduction activity of the $Fe(OH)_3/Fe_2O_3$@Au nanocomposite for 4-NP is because ultrathin $Fe(OH)_3/Fe_2O_3$ nanosheets have a large specific surface area. The simultaneous adsorption of 4-NP and BH_4^- on the catalyst is faster and more efficient, so the catalyst is quicker.

Finally, the effects of different precious metals additions (15 μmol L^{-1} Au, 10 μmol L^{-1} Au + 5 μmol L^{-1} Pt, 5 μmol L^{-1} Au + 10 μmol L^{-1} Pt and 15 μmol L^{-1} Pt) on the reduction activity of 4-NP were explored (as shown in Fig. 5d). However, no matter what kind of catalyst is used, the reaction does not occur immediately as soon as the catalyst is added. Instead, there is a plateau. Compared with the Au and Au–Pt sites, BH_4^- has a lower activation barrier for the adsorption and dissociation of Pt.[26,58] Therefore, as the Au content increases, the induction period is prolonged. As we can see from Fig. 5d, the composition of the catalyst is the main reason for the difference in the catalytic activity. The results show that $Fe(OH)_3/Fe_2O_3$@Au has the highest activity. In the process of $Fe(OH)_3/Fe_2O_3$@Au catalysis, the concentration of Au is only one-tenth or less than other similar catalysts. It is also more active than the Au–Pt alloy nanocube or Au–Pt alloy nanocomposite.[59] The results show that the $Fe(OH)_3/Fe_2O_3$@Au catalyst has extremely high catalytic activity, and a low concentration of Au can achieve high catalytic activity.

Stability and recyclability of the $Fe(OH)_3/Fe_2O_3$@Au composite nanocatalyst

A major advantage of the $Fe(OH)_3/Fe_2O_3$@Au composite catalyst is that the catalytic 4-NP reduction reaction can occur cyclically in the presence of $NaBH_4$. In order to avoid the loss of catalyst during the separation process, a cycle test was carried out on site. That is, 20 μL of the 4-NP solution was directly added to the reaction system after each reaction, and then the next test was performed. The synthesis conditions of the selected $Fe(OH)_3/Fe_2O_3$@Au composite catalyst are the optimized conditions of the above steps: 200 mg MES, 7 mg $FeSO_4$, 0.5 mg $NaBH_4$, and single metal Au. After three cycles, 4-NP can be completely reduced, but the catalytic activity is weakened. We will continue to improve this point in future experiments (as shown in Fig. 6). The morphology change after three cycles was also not obvious (Fig. S4†), indicating that the prepared $Fe(OH)_3/Fe_2O_3$@Au nanocomposite has excellent stability.

Conclusions

In this study, an ultrathin $Fe(OH)_3/Fe_2O_3$@Au composite catalyst has been synthesized by a green one-step method. The catalytic performance for 4-NP reduction under different conditions was investigated. The results show that MES will affect the dispersion of $Fe(OH)_3/Fe_2O_3$ nanosheets, and the size and distribution of Au nanoparticles. Simultaneously, the platform-time and catalytic efficiency of the $Fe(OH)_3/Fe_2O_3$@Au nanocomposites are affected by different contents of $FeSO_4$ and $NaBH_4$. The results also show that $Fe(OH)_3/Fe_2O_3$ nanosheets loaded with Au nanoparticles have a better catalytic effect than when it is loaded with Pt nanoparticles and Au–Pt alloy nanoparticles. By comparison, it was found that $Fe(OH)_3/Fe_2O_3$ nanosheets loaded with single metal Au nanoparticles have the highest catalytic activity. Furthermore, the $Fe(OH)_3/Fe_2O_3$@Au nanocomposite has good catalytic activity and stability for the catalytic reduction of 4-NP. We hope that our work can be used to prepare sustainable catalysts for the assembly of various metal nanoparticles with $Fe(OH)_3/Fe_2O_3$ nanosheets for advanced organic and pharmaceutical reduction processes.

Conflicts of interest

The authors declare no competing financial interest.

Acknowledgements

The authors are grateful for financial aid from the National Natural Science Foundation of China (Grant No. 21961001 and 32060549), and the Scientific research start-up funds for openly-recruited doctors provided by Gansu Agricultural University (GAU-KYQD-2018-14).

Notes and references

1 G. X. Wang, W. Chen, G. L. Chen, H. Jun, C. S. Song, D. L. Chen, Y. Du, C. R. Li and K. Ostrikov, *Nano Energy*, 2020, **71**, 104637.
2 J. Y. Fu, J. Lym, W. Q. Zheng, K. Alexopoulos, A. Mironenko, N. Li, J. Boscoboinik, D. Su, R. T. Weber and D. G. Vlachos, *Nat. Catal.*, 2020, **3**, 446.
3 S. Gao, H. Chen, Y. P. Liu, G. D Li, R. Q. Gao and X. X. Zou, *Inorg. Chem. Front.*, 2019, **6**, 940.
4 S. Y. Lu, H. Wu, S. Y. Xu, Y. K. Wang, J. Y. Zhao, Y. H. Li, A. M. Abdelkader, J. Li, W. Wang, K. Xi, Y. Z. Guo, S. J. Ding, G. X. Gao and R. Kumar, *Small*, 2021, **17**, 2005745.
5 D. L. Chen, Z. M. Xu, W. Chen, G. J. Chen, J. Huang, C. S. Song, K. Zheng, Z. X. Zhang, X. P. Hu, H. Choi and K. Ostrikov, *Small*, 2020, **16**, 2004843.
6 K. Goulas, A. Mironenko, G. Jenness, T. Mazal and D. Vlachos, *Nat. Catal.*, 2019, **2**, 269.
7 L. DeRita, J. Resasco, S. Dai, A. Boubnov, H. V. Thang, A. S. Hoffman, I. Ro, G. W. Graham, S. R. Bare, G. Pacchioni, X. Q. Pan and P. Christopher, *Nat. Mater.*, 2019, **18**, 746.

8 K. L. Zhang, Y. H. Li, S. J. Deng, S. H. Shen, Y. Zhang, G. X. Pan, Q. Q. Xiong, Q. Liu, X. H. Xia, X. L. Wang and J. P. Tu, *ChemElectroChem*, 2019, **6**, 3530.
9 X. J. Ni, J. F. Hao, Y. Q. Zhao, C. Yang, P. D. Sun, C. X. Wang and Y. X. Li, *Inorg. Chem. Front.*, 2017, **4**, 1634.
10 M. C. Luo, Z. L. Zhao, Y. L. Zhang, Y. J. Sun, Y. Xing, F. Lv, Y. Yang, X. Zhang, S. Hwang, Y. N. Qin, J. Y. Ma, F. Lin, D. Su, G. Lu and S. J. Guo, *Nature*, 2019, **574**, 81.
11 Y. L. Xu, X. F. Shi, R. Hua, R. Zhang, Y. J. Yao, B. Zhao, T. Liu, J. D. Zheng and G. Lu, *Appl. Catal. B Environ.*, 2020, **260**, 118142.
12 T. Braman, L. Dolvin, C. Thrasher, H. M. Yu, E. Q. Walhout and R. E. O'Brien, *Environ. Sci. Technol. Lett.*, 2020, **7**, 248.
13 C. Zhang, S. Govindaraju, K. Giribabu, Y. S. Huh and K. Yun, *Sens. Actuators, B*, 2017, **252**, 616.
14 L. R. Shultz, L. Hu, K. Preradovic, M. J. Beazley, X. F. Feng and T. Jurca, *ChemCatChem*, 2019, **11**, 2560.
15 T. Aditya, A. Pal and T. Pal, *Chem. Commun.*, 2015, **51**, 9410.
16 P. X. Zhao, X. W. Feng, D. S. Huang, G. Y. Yang and D. Astruc, *Coord. Chem. Rev.*, 2015, **287**, 114.
17 M. Chen, B. H. Wu, J. Yang and N. F. Zheng, *Adv. Mater.*, 2012, **24**, 862.
18 C. M. Piqueras, V. Puccia, D. A. Vega and M. A. Volpe, *Appl. Catal. B Environ.*, 2016, **185**, 265.
19 Q. N. Jiang, Z. Y. Jiang, L. Zhang, H. X. Lin, N. Yang, H. Li, D. Y. Liu, Z. X. Xie and Z. Q. Tian, *Nano Res.*, 2011, **4**, 612.
20 U. K. Arif, U. Sadeeq, P. Y. Qi, A. Shafqat, A. Aftab, U. H. Zia and U. R. Aziz, *Appl. Nanosci.*, 2020, **10**, 3901.
21 W. Ahmad, A. U. Khan, S. Shams, L. Qin, Q. P. Yuan, A. Ahmad, Y. Wei, Z. H. Khan, S. Ullah and A. U. Rahman, *J. Photochem. Photobiol. B Biol.*, 2020, **205**, 111821.
22 S. Shams, A. U. Khan, Q. P. Yuan, W. Ahmad, Y. Wei, Z. H. Khan, S. Shams, A. Ahmad, A. U. Rahman and S. Ullah, *J. Photochem. Photobiol. B Biol.*, 2019, **199**, 111632.
23 J. Zhang, S. F. Lu, Y. Xiang and S. P. Jiang, *ChemSusChem*, 2020, **13**, 2484.
24 F. Saira, N. Firdous, R. Qureshi and A. Ihsan, *Turk. J. Chem.*, 2020, **44**, 448.
25 H. R. Cho, Y. M. Kwon, Y. J. Lee, Y. A. Park, H. G. Ji and J. H. Lee, *Appl. Clay Sci.*, 2018, **156**, 187.
26 Y. Long, J. Li, L. L. Wu, J. Q. Li, X. Wang, S. Yao, S. Y. Song and H. J. Zhang, *Eur. J. Inorg. Chem.*, 2017, **1**, 146.
27 J. Z. Li, X. F. Bai and H. F. Lv, *Ultrason. Sonochem.*, 2020, **60**, 104746.
28 G. Z. Chen, Y. Wang, Y. W. Wei, W. Zhao, D. W. Gao, H. X. Yang and C. C. Li, *ACS Appl. Mater. Interfaces*, 2018, **10**, 11595.
29 X. T. Zuo, S. L. Ma, Q. Y. Wu, J. Xiong, J. J. He, C. Ma and Z. B. Chen, *J. Hazard. Mater.*, 2021, **411**, 125072.
30 H. Chen, Z. L. Zhang, D. M. Hu, C. H. Chen, Y. X. Zhang, S. J. He and J. L. Wang, *Chemosphere*, 2021, **265**, 129047.
31 H. Chen and J. L. Wang, *J. Hazard. Mater.*, 2020, **403**, 123697.
32 F. M. Valadi and M. R. Gholami, *J. Environ. Chem. Eng.*, 2021, **9**, 105408.
33 A. N. Chishti, F. Guo, A. Aftab, Z. Y. Ma, Y. Liu, M. Chen, J. Gautam, C. Chen, L. B. Ni and G. W. Diao, *Appl. Surf. Sci.*, 2021, **546**, 149070.
34 M. T. Alula, P. Lemmens, M. Madiba and B. Present, *Cellulose*, 2020, **27**, 2279.
35 M. Lashanizadegan, M. Anafcheh, H. Mirzazadeh and P. Gholipoor, *Mater. Res. Bull.*, 2020, **125**, 110773.
36 M. Yurderi, A. Bulut, G. S. Kanberoglu, M. Kaya, Y. Kanbur and M. Zahmakiran, *ChemistrySelect*, 2020, **5**, 6961.
37 J. W. Zhang and X. Zhang, *J. Alloys Compd.*, 2020, **842**, 155934.
38 S. J. Yang, J. Jeong, Y. M. Lim and J. S. Park, *Mater. Des.*, 2021, **201**, 109485.
39 T. Kavitha, I. K. Kang and S. Park, *Polym. Int.*, 2015, **64**, 1660.
40 H. M. Yang, S. B. Hong, Y. S. Choi, K. Lee, B. Seo and J. Moon, *J. Nanosci. Nanotechnol.*, 2016, **16**, 10864–10868.
41 P. J. Huang, J. Yang, K. Chong, Q. Y Ma, M. Li, F. Zhang, W. J. Moon, G. M. Zhang and J. W. Liu, *Chem. Sci.*, 2020, **11**, 6795.
42 H. Fan, X. Huang, L. Shang, Y. T. Cao, Y. F. Zhao, L. Z. Wu, C. H. Tung, Y. D. Yin and T. R. Zhang, *Angew. Chem.*, 2016, **55**, 2167.
43 W. L. Jia, F. P. Tian, M. J. Zhang, X. Y. Li, S. Ye, Y. F. Ma, W. Y. Wang, Y. F. Zhang, C. G. Meng, G. Zeng and J. Liu, *J. Colloid Interface Sci.*, 2021, **594**, 254.
44 M. Marimuthu, H. H. Li and Q. S. Chen, *J. Mol. Liq.*, 2021, **333**, 115963.
45 R. Ghorbani-Vaghei, H. Veisi, M. H. Aliani, P. Mohammadi and B. Karmakar, *J. Mol. Liq.*, 2020, **327**, 114868.
46 Y. G. Li, X. J. Quan, C. Y. Hu and C. P. Li, *ACS Appl. Energy Mater.*, 2020, **3**, 4756.
47 M. T. Alula, P. Lemmens and M. L. Madingwane, *Microchem. J.*, 2020, **156**, 104976.
48 T. T. Bui, Y. Kim, S. Kim and H. Lee, *RSC Adv.*, 2015, **5**, 75272.
49 V. Nesterov, D. Reiter, P. Bag, P. Frisch, R. Holzner, A. Porzelt and S. Inoue, *Chem. Rev.*, 2018, **118**, 9678.
50 A. A. Kassem, H. N. Abdelhamid, D. M. Fouad and S. A. Ibrahim, *J. Environ. Chem. Eng.*, 2020, **9**, 2213.
51 J. Strachan, C. Barnett, A. F. Masters and T. Maschmeyer, *ACS Catal.*, 2020, **10**, 5516.
52 Q. Ding, Z. W. Kang, L. P. Cao, M. S. Lin, H. T. Lin and D. P. Yang, *Appl. Surf. Sci.*, 2020, **510**, 145526.
53 V. Balakumar, H. Kim, J. W. Ryu, R. Manivannan and Y. Son, *J. Mater. Sci. Technol.*, 2020, **40**, 178.
54 X. Y. Huang, L. Chang, Y. G. Lu, Z. H. Li, Z. W. Kang, X. H. Zhang, M. H. Liu and D. P. Yang, *Mater. Sci. Eng. C*, 2020, **113**, 111015.
55 P. H. Fraijo, E. Smolentseva, A. Simakov, M. José-Yacaman and B. Acosta, *Microporous Mesoporous Mater.*, 2020, **312**, 110707.
56 A. Zhou, J. Z. Li, G. H. Wang and Q. H. Xu, *Appl. Surf. Sci.*, 2019, **506**, 144570.
57 C. Du, S. J. He, X. H. Gao and W. Chen, *ChemCatChem*, 2016, **8**, 2885.
58 J. M. Zhang, G. Z. Chen, D. Guay, M. Chaker and D. L. Ma, *Nanoscale*, 2014, **6**, 2125.
59 G. T. Fu, L. F. Ding, Y. Chen, J. Lin, Y. W. Tang and T. H. Lu, *CrystEngComm*, 2014, **16**, 1606.